RSC Advances

PAPER

View Article Online
View Journal | View Issue

Cite this: *RSC Adv.*, 2022, **12**, 1922

Phosphonium-based ionic liquids as antifungal agents for conservation of heritage sandstone†

Qiang Li,*[a] Yulan Hu[a] and Bingjian Zhang *[ab]

Received 19th December 2021
Accepted 3rd January 2022

DOI: 10.1039/d1ra09169g

rsc.li/rsc-advances

With a view to preventing fungal deterioration of historical stone artworks, we report the use of phosphonium-based ionic liquids (ILs) as potent antifungal agents against dematiaceous fungi commonly found on heritage stones. Three ILs: tributyldodecylphosphonium polyoxometalate $[P_{44412}][POM]$, tributyltetradecylphosphonium polyoxometalate $[P_{44414}][POM]$, and trihexyltetradecylphosphonium polyoxometalate $[P_{66614}][POM]$ were prepared and their thermal stabilities and *in vitro* antifungal activities were evaluated. From the ramped temperature thermogravimetric analysis and antifungal experiments it can be clearly observed that the alkyl chain length of the tetraalkylphosponium cation has a significant influence on the thermal and antifungal properties. The thermal stability and antifungal activity decreased as the number of carbon atoms of the alkyl substituents increased and, thus, followed the order $[P_{44412}][POM]$ > $[P_{44414}][POM]$ > $[P_{66614}][POM]$. In addition, inoculation of four fungal species on IL-coated sandstone surfaces showed significant inhibition of fungal growth, endowing the materials with potential applications in heritage sandstone conservation.

1. Introduction

The essential roles of fungal communities in the process of heritage stone deterioration are well known.[1–3] Different fungal species are mainly associated with the active biodeterioration process, thereby resulting in aesthetic and structural impairment of cultural heritage.[4,5] One of the most evident signs of aesthetic appearance issues is the colonization of melanin-producing dematiaceous fungi.[6–8] These dematiaceous fungi are not only able to survive under adverse environmental conditions,[9,10] but also may serve as potential human and plant pathogens.[11] Moreover, melanized fungal cells may resist killing by antibiotics or other anti-microbial treatments.[12,13] Some commercially available chemical products have been widely used to inhibit or eliminate fungal growth.[14–16] These methods do exhibit significant disadvantages,[17,18] however, like their harmfulness to humans and the environment, their limited long-term efficiency, and their unwanted negative effects on stone monuments. A large number of novel biocides based on nanomaterials and natural compounds appear very promising to prevent the biodeterioration of historical stone materials.[19,20] Nevertheless, further studies are really needed to evaluate their potentially hazardous effects, antifungal efficiency, and durability.[21,22]

Ionic liquids (ILs) as an innovative class of nonmolecular, tuneable, and remarkable chemical compounds, have applied in many areas of modern science.[23] In the field of cultural heritage conservation, ILs have been successfully used for the removal of corrosion crusts and varnish from cultural heritage surfaces.[24,25] Moreover, ILs are also being considered as antibacterial and antifungal agents,[26] and have been widely exploited for preserving wood,[27,28] paper,[29,30] stone,[31,32] and brick[33] heritages against biodeterioration. The organic cations, typically imidazolium, alkylammonium, and alkylphosphonium, contribute to their superior antimicrobial activities.[34] Meanwhile, the biocidal activity is greatly affected by the alkyl chain length and positive charge density of cations, in which the higher charge density or moderate side chain length results in improved antimicrobial activity.[35,36] The anions, including simple halides, and organic and inorganic species, usually are employed to tune the physicochemical properties and play a significant role in the design of multifunctional ILs.[37] Polyoxometalates (POMs) are a family of inorganic metal oxygen anion clusters and have received significant interest because of their redox and topological properties.[38] Bijelic *et al.* focused on the antibacterial activity of POMs and underlined that POMs can also directly interact with proteins and enzymes, leading to serious damage within the bacterial cell.[39] Herrmann *et al.* designed a polyoxometalate supported ionic liquid phase (POM-SILP) composite for the removal of multiple contaminants from water, and results indicate that the multi-functional composite can effectively remove toxic heavy metals and organic pollutants.[40] Regarding the application of POMs-based ILs for the protection of cultural artifacts, to our knowledge, limited work

[a]*School of Art and Archaeology, Zhejiang University, Hangzhou, Zhejiang 310058, China. E-mail: zhangbiji@zju.edu.cn; 11437071@zju.edu.cn*

[b]*Department of Chemistry, Zhejiang University, Hangzhou, Zhejiang 310027, China*

† Electronic supplementary information (ESI) available. See DOI: 10.1039/d1ra09169g

has been done.[33] Misra *et al.* reported a multifunctional POM-ILs transparent coating for natural stones, and results show that the coating protects the stone surfaces from acid corrosion and bacterial colonization.[41]

Considering the structural stability of POM anion and high positive charge of tetraalkylphosphonium cation, we designed to synthesize three ILs, namely $[P_{44412}][POM]$, $[P_{44414}][POM]$, and $[P_{66614}][POM]$, respectively (Fig. 1), aiming to prevent fungal contamination of stone surfaces. Phosphonium-based POM-ILs may possess higher thermal stability in comparison with its ammonium analogue.[42,43] Moreover, improved antimicrobial activity could also be achieved since the phosphorus atom has larger atomic radius and lower electronegativity, preferential binding to the negatively charged cell membrane and killing them.[44–46]

2. Materials and methods

2.1 Materials

Tributyldodecylphosphonium bromide was purchased from Titan Biotech Co. Ltd. (Shanghai, China) with a purity of 98%. Dimethyl sulfoxide (DMSO), $Na_2WO_4 \cdot 2H_2O$, $Na_2SiO_3 \cdot 5H_2O$, toluene, chloroform, tributyltetradecylphosphonium chloride (50% in water, Macklin), and trihexyltetradecylphosphonium chloride (97%, Macklin) were obtained from Shanghai Macklin Biochemical Co., Ltd. (Shanghai, China). Fluconazole and XTT (2,3-bis(2-methoxy-4-nitro-5-sulfophenyl)-2*H*-tetrazolium-5-carb oxanilide, sodium salt) were obtained from Yuanye Biotech Co. Ltd. (Shanghai, China). RPMI 1640 medium without sodium bicarbonate, with L-glutamine, was purchased from Sigma. Four dematiaceous fungi, which were isolated from contaminated historical buildings and identified as *Curvularia* sp. F3, *Aspergillus aculeatinus* F6 (*A. aculeatinus* F6), *Aporospora* sp. F7, and *Alternaria* sp. F8, were used as test fungi in the experiments.

2.2 Synthesis and characterization of ILs

Three phosphonium-based ILs were synthesized according to procedures reported previously.[41,47] Briefly, 5 g of $K_8[\alpha\text{-}SiW_{11}O_{39}] \cdot 13H_2O$ was dissolved in 100 mL of water and then the mixture was stirred at 50 °C until completely dissolution. Subsequently, 1.55 mmol of the corresponding tetraalkylphosponium salt (dissolved in 100 mL of toluene) was added to the first solution. The resulting biphasic solution was stirred vigorously for 25 min. After this time, the layers were separated, and the aqueous phase was extracted with toluene. The combined organic layers were evaporated under reduced pressure and the resulting light-yellow highly viscous liquid was washed once with toluene and twice with chloroform, and then dried under vacuum at room temperature for 96 h.

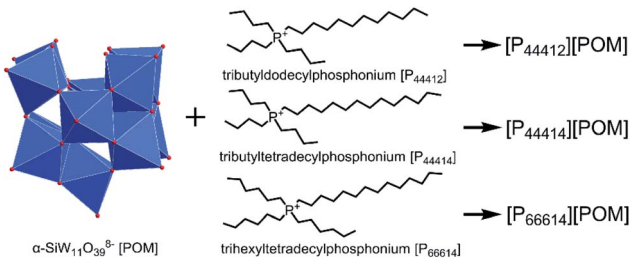

Fig. 1 Schematic illustration of the $[P_{44412}][POM]$, $[P_{44414}][POM]$, and $[P_{66614}][POM]$.

The elemental composition of $K_8[\alpha\text{-}SiW_{11}O_{39}] \cdot 13H_2O$ was determined using inductively coupled plasma atomic emission spectrometry (ICP-AES, Thermo iCAP 6300). The elemental composition (C and H) of the three ILs was assayed on an Elementar Vario Micro Cube instrument. Fourier transform infrared (FTIR) spectra of the prepared ILs were recorded on a Thermo Scientific Nicolet iS10 spectrometer. Thermal gravimetric analysis (TGA) was performed on a Netzsch STA409PC instrument under nitrogen conditions, with a heating rate of 10 °C min^{-1} in the temperature range of 25–600 °C. Proton nuclear magnetic resonance (^1H NMR) spectra were recorded on a Bruker AVANCE III 500 MHz spectrometer. ^1H NMR ($CDCl_3$, δ) for $[P_{44412}][POM]$: δ 2.65–2.31 (m, 8H), 1.71–1.41 (m, 16H), 1.26 (s, 16H), 0.92 (dt, J = 41.3, 6.9 Hz, 12H). ^1H NMR ($CDCl_3$, δ) for $[P_{44414}][POM]$: δ 2.60–2.32 (m, 8H), 1.57 (dq, J = 7.6, 3.7 Hz, 16H), 1.26 (s, 20H), 0.92 (dt, J = 39.2, 6.8 Hz, 12H). ^1H NMR ($CDCl_3$, δ) for $[P_{66614}][POM]$: δ 2.63–2.27 (m, 8H), 1.69–1.45 (m, 16H), 1.44–1.15 (m, 32H), 0.88 (td, J = 7.0, 3.1 Hz, 12H).

2.3 *In vitro* assessment of antifungal activities of ILs

A disk diffusion assay was performed to determine the antifungal efficacy of different concentrations of ILs. Briefly, 150 μL each of the conidial and mycelial suspensions was spread on potato dextrose agar (PDA) plates using a sterile glass spreader. Seven cylindrical wells with diameters of 7.5 mm were radially punched in the agar plate with a stainless-steel cylinder. Each well was filled with 100 μL of the as-prepared ILs dissolved in DMSO to obtain different concentrations 0.05, 0.1, 0.5, 1, 5, and 10 mg mL^{-1}. The well without ILs served as a negative control and fluconazole served as a positive control. The plates were incubated at 30 °C for 48 h and the inhibition diameter was calculated to evaluate the antifungal activities of the corresponding ILs. All assays were performed in triplicate.

A colony biofilm formation test was performed on agar plates supplemented with different concentrations of ILs. Briefly, all the synthesized ILs were dissolved in DMSO and mixed with a sterile molten PDA medium to achieve final concentrations of 0.05, 0.1, 0.5, 1, 5, and 10 mg mL^{-1}. The PDA medium with a final concentration of 1% DMSO (v/v) was used as a control. The mycelial disks (5 mm in diameter) of isolated fungi were inoculated on PDA plates and then incubated at 30 °C for 3 d. All experiments were repeated three times. The percentage reductions in the biofilm were calculated according to the following formula:

$$\text{Biofilm reduction ratio (\%)} = [(C - T)/(C - 5\ \text{mm})] \times 100,$$

where C and T are the diameters of the fungal biofilms of the control and treatment samples, respectively. XTT-reduction assay was used to determine the *in vitro* activities of the ILs against fungal biofilms (ESI Methods 1.1†).[48] All experiments were performed in triplicate.

2.4 Propidium iodide uptake assay and scanning electron microscope observations

The fungal membrane permeabilization and cell viability were studied using a propidium iodide (PI) uptake assay. Briefly, fungi were inoculated into 50 mL of potato dextrose broth and grown at 30 °C for 4 d with vigorous shaking (160 rpm). Subsequently, the culture was washed with phosphate-buffered saline (PBS) three times and transferred to a 24-well plate wherein each well contained a mixture of RPMI 1640 medium and ILs. Final concentrations of 0.1 and 1 mg mL^{-1} were set up for each IL, and the well containing 1% DMSO served as a control. The cell suspensions were then incubated at 30 °C for 12 h with continuous shaking (150 rpm). After incubation, the cell suspensions were centrifuged and washed twice in PBS. Staining was detected using a fluorescence microscope (Olympus CX41) after fungal cells were stained with PI for 30 min at room temperature.

A fluorescence-based test was also conducted to determine the fungal cell viability on simulated sandstone samples (diameter, 20 mm; height, 8 mm) coated with three ILs. Sandstone samples were prepared according to procedures reported previously.[49] Twelve samples were coated with $[P_{44412}][POM]$, $[P_{44414}][POM]$, and $[P_{66614}][POM]$, respectively (10 mg mL^{-1} of IL dissolved in acetone, ~3.18 mg cm^{-2} per sample), and an additional four samples were left uncoated. All samples were placed in an oven at 55 °C for 2 h to allow the evaporation of the solvent, thereby yielding a thin IL layer. The fungal inoculum was deposited on sandstone surfaces and incubated in an incubator with a constant climate of 30 °C and 80% relative humidity for 10 d. All samples were directly stained with PI and the generated biofilm was visualized on a fluorescence microscope. Additionally, the fungal morphology was observed using scanning electron microscope (SEM).

The color parameters of CIE $L^*a^*b^*$ were determined using a colorimeter Konica Minolta CR-10. The simulated sandstone samples were measured before and after treatment with the ILs. The total colorimetric change was determined by ΔE, which was calculated by following equation:

$$\Delta E = \sqrt{(\Delta L^*)^2 + (\Delta a^*)^2 + (\Delta b^*)^2},$$

where, ΔL^*, Δa^*, and Δb^* are the luminosity change, red-green parameter, and blue-yellow parameter, respectively.

3. Results and discussion

3.1 Structural analysis of three ILs and their thermal stabilities

The structures of the obtained ILs were characterized by elemental analysis, FTIR, and ^1H NMR spectroscopy. The carbon contents of $[P_{44412}][POM]$, $[P_{44414}][POM]$, and $[P_{66614}][POM]$ are 41.51%, 42.82%, and 45.86%, respectively which are

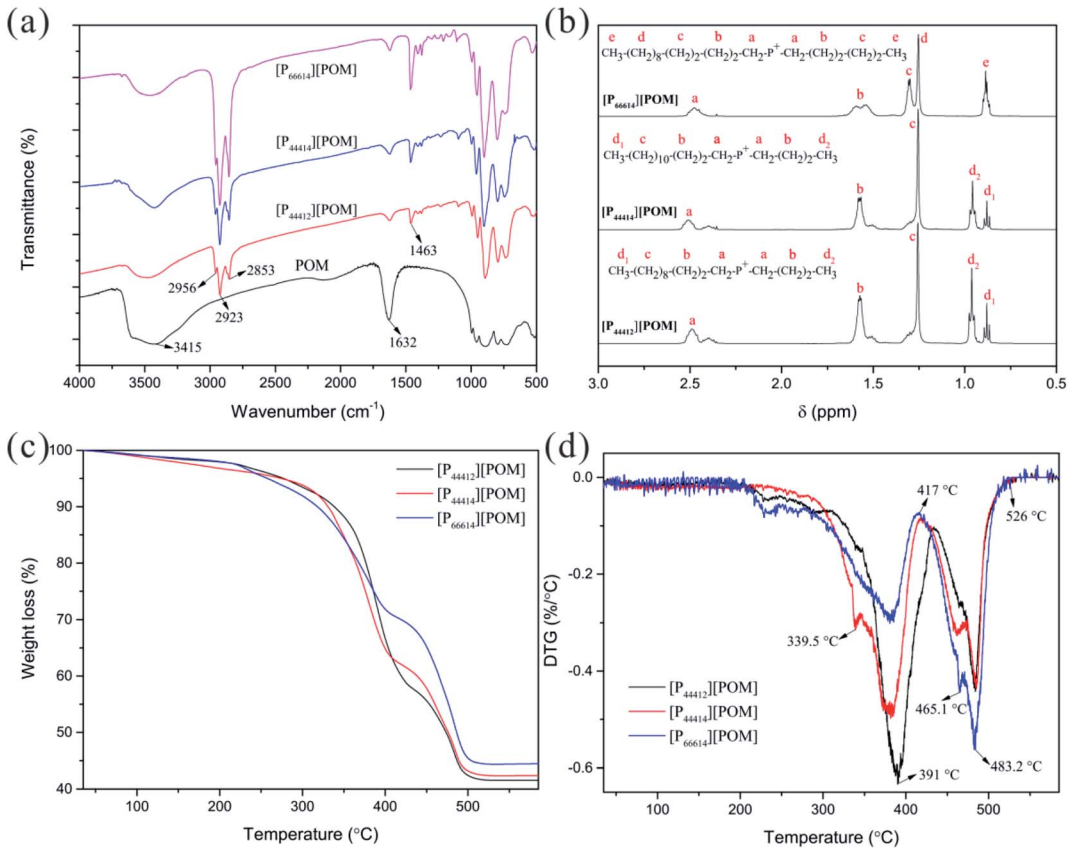

Fig. 2 Characterization of $[P_{44412}][POM]$, $[P_{44414}][POM]$, and $[P_{66614}][POM]$. FTIR (a) and ^1H NMR (b) spectra of ILs. TGA (c) and DTG (d) curves of ILs.

more likely somewhere near the corresponding calculated values of 40.82%, 42.53%, and 46.97%. As expected, the hydrogen contents of the ILs synthesized in this work correspond to the actual values (Table S1†). The FTIR spectra of the three ILs are shown in Fig. 2a, together with the spectrum of the POMs. A decrease in the absorption peak intensity at 3415 and 1632 cm^{-1} is observed in the three ILs, suggesting that little water is present in the ILs. Three bands are observed at 2956, 2923, and 2853 cm^{-1}, which are attributed to the presence of $-CH_3$ and $-CH_2$ groups. Meanwhile, three ILs present the new characteristic band at 1463 cm^{-1} which are assigned to P–CH_2 vibration.[50,51] The structure of the ILs is also confirmed by ^1H NMR spectroscopy. As shown in Fig. 2b, the NMR signals correspond to the tetraalkylphosponium groups. Therefore, it is concluded that the three ILs are synthesized successfully.

TGA of the three ILs was performed under an N_2 atmosphere, from room temperature to 600 °C. The TGA spectra of the ILs and its derivative curves are shown in Fig. 2c and d, respectively. For three ILs, weight loss is seen to occur in three stages. In the temperature range from room temperature to 200 °C, weight losses of 2.1%, 3.2%, and 2% are observed for the $[P_{44412}][POM]$, $[P_{44414}][POM]$, and $[P_{66614}][POM]$, respectively, which are attributed to the evaporation of water. The second stage, more significant losses for the $[P_{44412}][POM]$, $[P_{44414}][POM]$, and $[P_{66614}][POM]$ occur at 350.5 °C (T_{onset}; T_{max} = 391 °C), 335.8 °C (T_{onset}; T_{max} = 382.6 °C), and 308.3 °C (T_{onset}; T_{max} = 381.2 °C), respectively, these onset temperatures consistent with literature reports indicating thermal stabilities of many phosphonium-based ILs exceeding 300 °C.[43] Apparently, increasing the alkyl chain length decreases the decomposition temperature and thermal stability, and the same trend is observed in a series of ILs,[52,53] which may be attributed to the increased stability of the carbocation and/or carbon radicals when the alkyl chain increases.[54,55] Moreover, it was clear that phosphonium-based POM-ILs are found to have a higher thermal stability than its ammonium analogue.[42,56] The third stage, decomposition of the organic and inorganic moieties into volatile products is essentially complete, with 41.6% (calc. 47.4%), 42.4% (calc. 45.6%), and 44.4% (calc. 40.9%) of the sample weight remaining for $[P_{44412}][POM]$, $[P_{44414}][POM]$, and $[P_{66614}][POM]$, respectively. It is of interest to note, although the

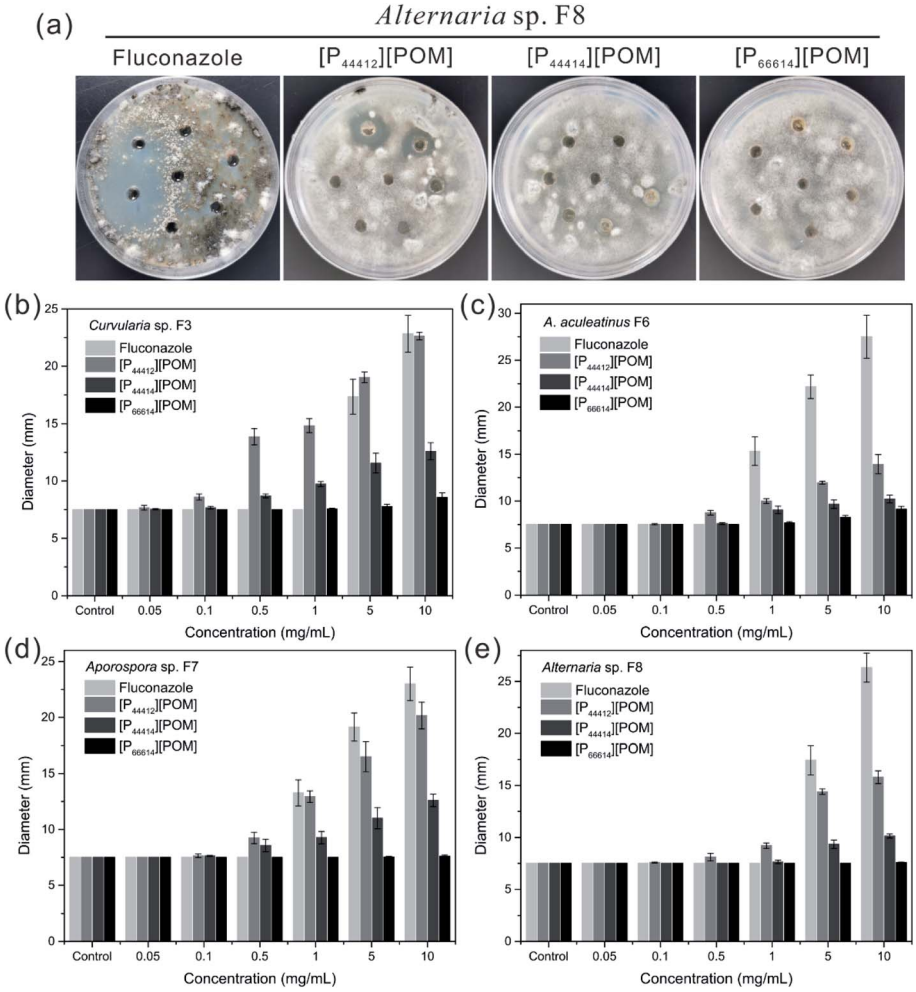

Fig. 3 Photographs (a) and the statistical histogram of the inhibition zones of (b) *Curvularia* sp. F3, (c) *A. aculeatinus* F6, (d) *Aporospora* sp. F7, and (e) *Alternaria* sp. F8 after treatment with different concentrations (0.05, 0.1, 0.5, 1, 5, and 10 mg mL^{-1}) of fluconazole, $[P_{44412}][POM]$, $[P_{44414}][POM]$, and $[P_{66614}][POM]$.

ramped temperature TGA method exhibits a wide working temperature range of three ILs, time consuming isothermal TGA analyses will be necessary to obtain more profound and accurate information on the thermal stability properties.[57]

3.2 Antifungal properties

The antifungal activities of $[P_{44412}][POM]$, $[P_{44414}][POM]$, and $[P_{66614}][POM]$ were determined by a disk diffusion method in terms of the zone of inhibition of fungal growth (Fig. 3a). Fig. 3b–e show the antifungal activities of different concentrations (0.05, 0.1, 0.5, 1, 5, and 10 mg mL^{-1}) of ILs and fluconazole against *Curvularia* sp. F3, *A. aculeatinus* F6, *Aporospora* sp. F7, and *Alternaria* sp. F8. Remarkably, *A. aculeatinus* F6, *Aporospora* sp. F7, and *Alternaria* sp. F8 are especially sensitive to the most common antifungal fluconazole and the diameter of the inhibition zone as high as 27.5 ± 2.3 mm is observed (Fig. 3c). However, for equal content of fluconazole and $[P_{44412}][POM]$, the antifungal activity of $[P_{44412}][POM]$ against *Curvularia* sp. F3 is stronger than that of fluconazole (Fig. 3b). $[P_{44412}][POM]$ exhibits an excellent antifungal efficacy compared to those of $[P_{44414}][POM]$ and $[P_{66614}][POM]$. At a concentration of 10 mg mL^{-1}, distinct inhibition halos appear for the $[P_{44412}][POM]$ group (~22.6 ± 0.3 mm for *Curvularia* sp. F3, ~13.9 ± 1.0 mm for *A. aculeatinus* F6, ~20.2 ± 1.2 mm for *Aporospora* sp. F7, and ~15.8 ± 0.6 mm for *Alternaria* sp. F8), which are larger than those of the $[P_{44414}][POM]$ group (~12.6 ± 0.7 mm for *Curvularia* sp. F3, ~10.2 ± 0.4 mm for *A. aculeatinus* F6, ~12.6 ± 0.6 mm for *Aporospora* sp. F7, and ~10.1 ± 0.2 mm for *Alternaria* sp. F8). In contrast, $[P_{66614}][POM]$ does not exhibit any evident inhibition zone against the four fungal isolates, which is likely due to its longer alkyl chains compared to those of the other two ILs. Specifically, there are no significant differences in the reduction rates of the control and treatment (0.05 and 0.1 mg mL^{-1}) groups, suggesting that the four fungi are less susceptible to lower doses of ILs.

Fig. 4 shows the inhibition ratios of the three ILs at different concentrations (0.05, 0.1, 0.5, 1, 5, and 10 mg mL^{-1}). For *Curvularia* sp. F3 (Fig. 4a), $[P_{44412}][POM]$ exhibits the highest antifungal activity compared to the other ILs at the same dosage. Even at a $[P_{44412}][POM]$ concentration of 0.05 mg mL^{-1}, the inhibitory ratio reaches 61.9%. In the case of *A. aculeatinus* F6 (Fig. 4b), $[P_{44412}][POM]$ shows the highest antifungal activity among the three target ILs, as expected, with 83.2% and 96% decreases in the fungal-colonized areas at concentrations of 0.5 and 10 mg mL^{-1}, respectively. However, a concentration of 1 mg mL^{-1} of $[P_{44414}][POM]$ or 10 mg mL^{-1} of $[P_{66614}][POM]$ is needed to achieve more than 80% cell death. In the case of *Aporospora* sp. F7, $[P_{44412}][POM]$ and $[P_{44414}][POM]$ shows similar antifungal activities when the concentrations of the ILs are lower than 1 mg mL^{-1}, even though the alkyl groups of the two ILs are different (Fig. 4c). In the assays of the three ILs against *Alternaria* sp. F8 (Fig. 4d), $[P_{44412}][POM]$ and $[P_{44414}][POM]$ exhibit a higher antifungal activity than does $[P_{66614}][POM]$. Even at a concentration of 0.1 mg mL^{-1} of $[P_{66614}][POM]$, the inhibitory

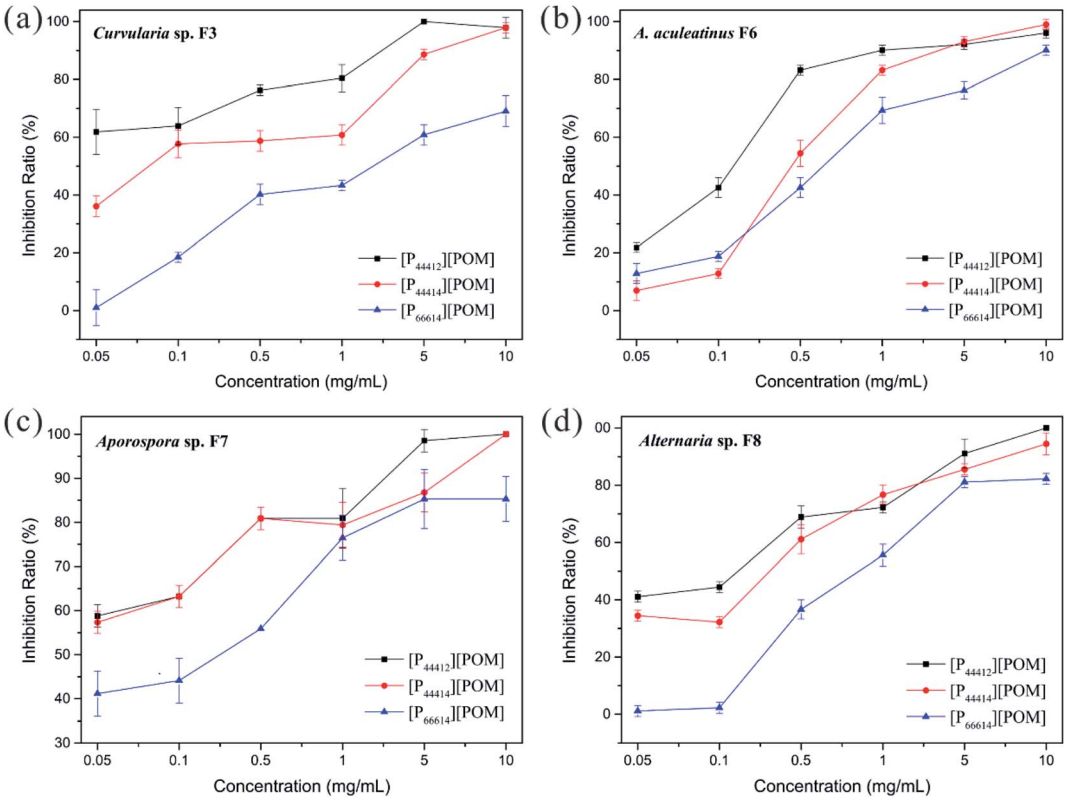

Fig. 4 Inhibition of biofilm formation at different concentrations (0.05, 0.1, 0.5, 1, 5, and 10 mg mL^{-1}) of $[P_{44412}][POM]$, $[P_{44414}][POM]$, and $[P_{66614}][POM]$: (a) *Curvularia* sp. F3, (b) *A. aculeatinus* F6, (c) *Aporospora* sp. F7, and (d) *Alternaria* sp. F8.

ratio is still 2.2%, whereas 44.4% and 32.2% reductions are observed for $[P_{44412}][POM]$ and $[P_{44414}][POM]$, respectively.

The results shown in Fig. 5 indicate that the metabolic activity of the fungal biofilm decreased gradually with the increase in the IL concentration. After treatment with $[P_{44412}][POM]$ and $[P_{44414}][POM]$ at a concentration of 0.1 mg mL^{-1}, *Curvularia* sp. F3 exhibits metabolic activities of approximately 52.95% and 56.51% compared with the control group, respectively, whereas a metabolic activity of 71.18% is observed in the $[P_{66614}][POM]$ group (Fig. 5a). In the *A. aculeatinus* F6 group, the metabolic activity of the biofilm shows no significant difference after incubation with the same doses of $[P_{44412}][POM]$, $[P_{44414}][POM]$, and $[P_{66614}][POM]$ (Fig. 5b). After treatment with $[P_{44412}][POM]$ and $[P_{44414}][POM]$ at concentrations of 0.05 mg mL^{-1}, the metabolic activity of *Aporospora* sp. F7 is reduced by 56% and 55.2%, respectively, and thus, these ILs exhibit a higher antifungal activity than that of $[P_{66614}][POM]$ (26%) (Fig. 5c). To achieve 50% growth inhibition of *Alternaria* sp. F8 with the control group, a concentration of 0.1–0.5 mg mL^{-1} is needed for $[P_{44412}][POM]$. However, in the $[P_{44414}][POM]$ and $[P_{66614}][POM]$ groups, the required concentration is higher than 0.5 mg mL^{-1} (Fig. 5d).

As shown in Fig. 3–5, the antifungal activities of each IL against four dematiaceous fungi are compared, the IL efficacy is in the following order: $[P_{44412}][POM] > [P_{44414}][POM] > [P_{66614}][POM]$. Interestingly, in the disk diffusion assay, only $[P_{44412}][POM]$ exhibits a strong inhibitory activity, while $[P_{66614}][POM]$ does not exhibit any evident inhibition zone, even at a high concentration (5 and 10 mg mL^{-1}). In the colony biofilm formation and XTT-reduction assays, $[P_{66614}][POM]$ is found to have high antifungal activity, especially when the $[P_{66614}][POM]$ concentration is higher than 0.5 mg mL^{-1}. The fact may be related to the strong electrostatic interaction between phosphonium cation and bulky POM anion limits the diffusion of antimicrobial cation species into the agar medium and subsequent delivery to microbial cells.[58] This conclusion is consistent with previous findings of Rajkowska *et al.*,[33] who assayed the antifungal activities of ammonium-based POM-ILs and each component alone and revealed that diffusion-based antifungal activities of POM-ILs arise primarily from the cation species. Additionally, it is clear that cationic biocides kill bacteria by binding to negatively charged cell surface and disrupting the cell membranes, in which different charge distributions and alkyl chain length play a key role in the antibacterial efficacy.[46,59] In this study, three phosphonium-based ILs with different long alkyl chains (C_{12} and C_{14}) exhibit antifungal activity, which is consistent with previous reports indicating that phosphonium compounds containing a long alkyl chain (C_8–C_{18}) usually exert antimicrobial capabilities.[45,60,61] Regarding the $[P_{44412}][POM]$ with a shorter alkyl chain, a high level of antifungal activity is

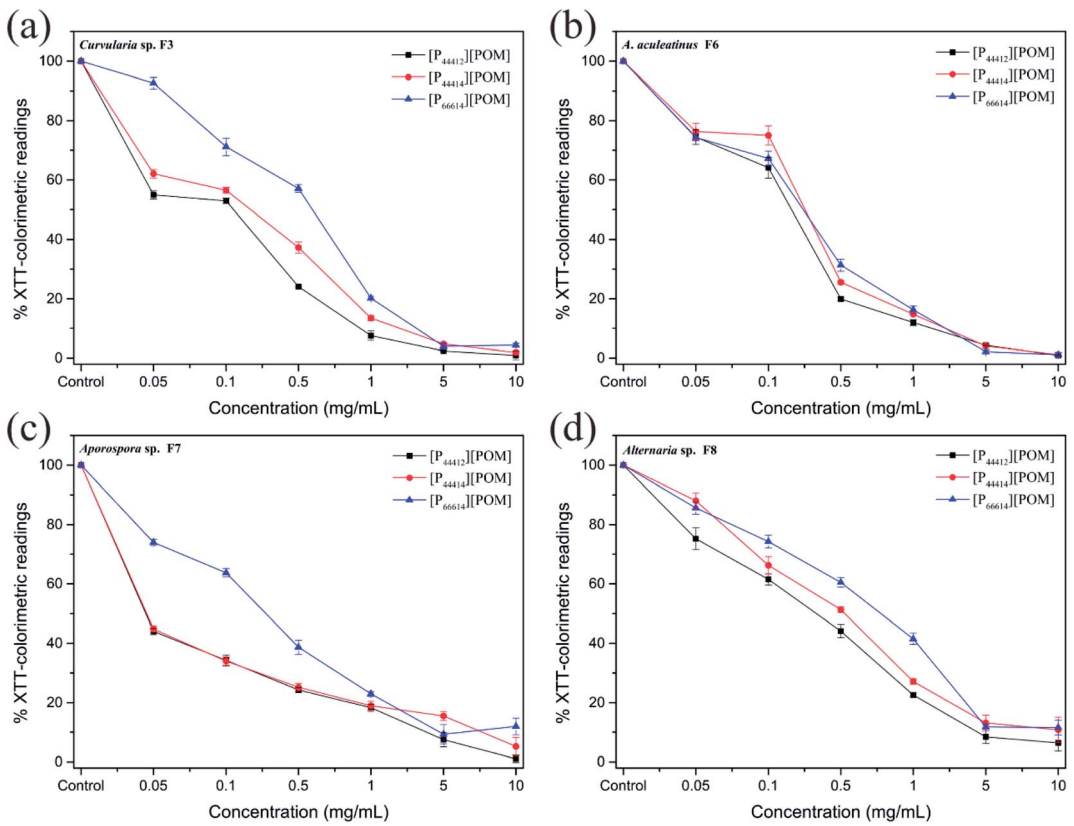

Fig. 5 Activities of different ionic liquid (IL) concentrations against pre-formed biofilms of (a) *Curvularia* sp. F3, (b) *A. aculeatinus* F6, (c) *Aporospora* sp. F7, and (d) *Alternaria* sp. F8. The average percentage XTT-colorimetric readings represent the biofilm metabolic activity compared to that of the control group.

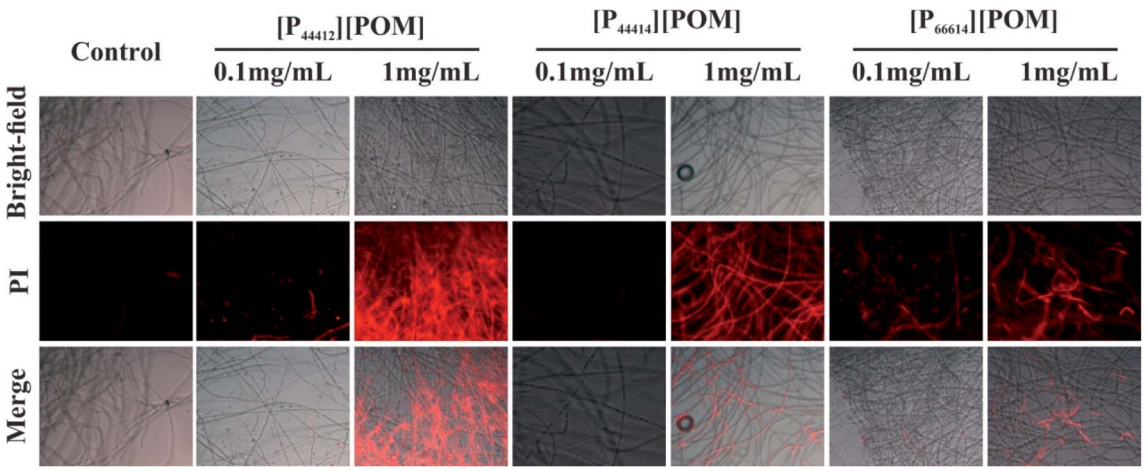

Fig. 6 Effect of ILs at concentrations of 0.1 and 1 mg mL^{-1} on the membrane integrity of *Curvularia* sp. F3.

observed, which may be affected by many potential important factors, such as hydrophobic-hydrophilic balance,[62,63] adsorption, and critical micelle concentration.[64]

Because phosphonium-based cations can adsorb negatively charged cell walls and membranes *via* electrostatic interactions and disrupt the cytoplasmic membrane *via* the hydrophobic alkyl chains,[44,46] thereby leading to cell death, PI fluorescent dye was used to evaluate the antifungal efficiencies of the three ILs. As shown in Fig. 6, almost no red fluorescence is present in the *Curvularia* sp. F3 incubated without ILs, suggesting that the fungal cell membrane remains intact. However, the fungi that are co-cultured with $[P_{44412}][POM]$, $[P_{44414}][POM]$, and $[P_{66614}][POM]$ displays red fluorescence, and the red fluorescence signal intensity of fungal cells incubated with 1 mg mL^{-1} ILs is significantly enhanced compared with the signal of the cells treated with 0.1 mg mL^{-1} ILs. The appearance of strong red fluorescence suggests that more fungal membranes are efficiently destroyed and that fungi are more sensitive to high concentrations of the ILs. Moreover, an increase in the fluorescence intensity, indicative of fungal cell death, is observed when the fungi are incubated with $[P_{44412}][POM]$ and $[P_{44414}][POM]$, which is consistent with the results of the antifungal experiments. The fluorescence images of *A. aculeatinus* F6, *Aporospora* sp. F7, and *Alternaria* sp. F8 further confirm the antifungal activities of the synthesized ILs (Fig. S1†).

To determine the antifungal effectiveness of the ILs that are applied to the simulated sandstone, the inhibition of the growth of *Curvularia* sp. F3, *A. aculeatinus* F6, *Aporospora* sp. F7, and *Alternaria* sp. F8 is studied using a fluorescence-based test. Fig. 7 shows the optical and fluorescence microscopy images of

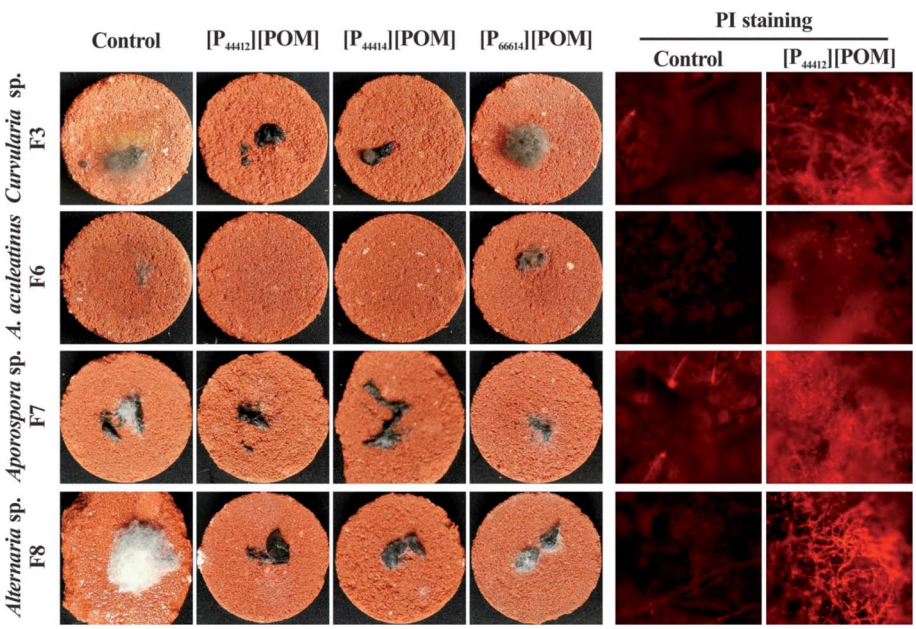

Fig. 7 Optical and fluorescence images of fungi incubated over sandstone samples coated with $[P_{44412}][POM]$, $[P_{44414}][POM]$, and $[P_{66614}][POM]$.

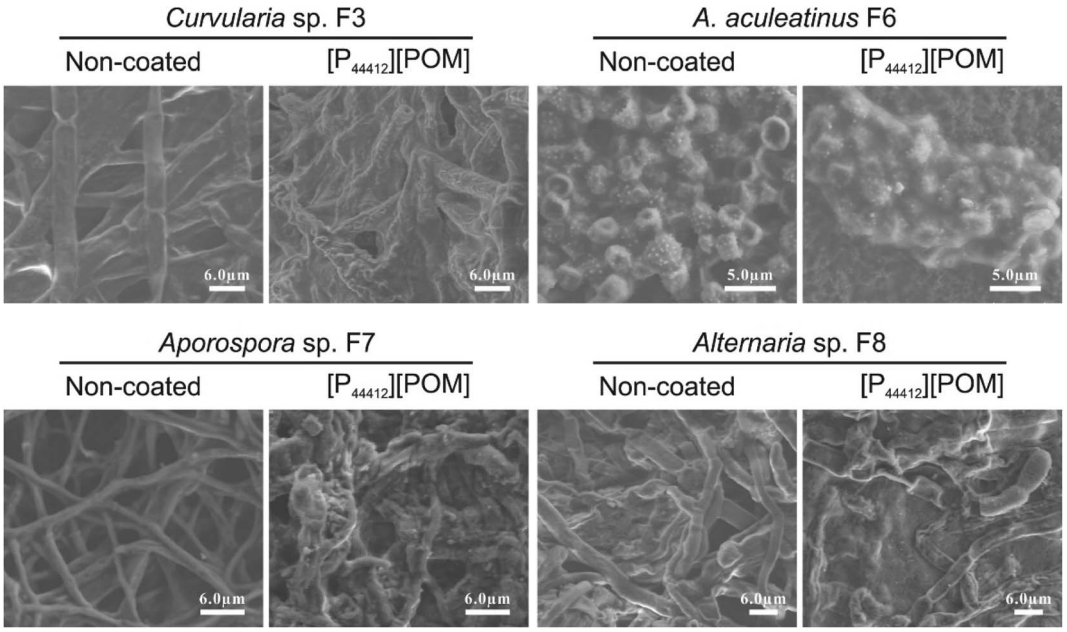

Fig. 8 SEM images of antifungal activity of $[P_{44412}][POM]$ on the sandstone samples.

the surfaces of the sandstone that are untreated and treated with the ILs after incubation with the four fungi. A significant increase of fungal growth over all untreated and $[P_{66614}][POM]$-treated sandstone samples is detected, whereas it is found that the coatings of $[P_{44412}][POM]$ and $[P_{44414}][POM]$ substantially decrease the fungal colonization. Red fluorescence is clearly detected on the surfaces coated with $[P_{44412}][POM]$, and weak fluorescence is observed on the non-coated samples, indicating a significant antifungal effectiveness on $[P_{44412}][POM]$ for both fungal species.

Fungi incubated over the $[P_{44412}][POM]$-coated sandstone were further examined by SEM and the typical images are displayed in Fig. 8. In control images, fungal spores and mycelium exhibit a normal shape with intact membranes/walls. In contrast, after exposure to $[P_{44412}][POM]$, significant cellular morphologic changes (smooth surfaces become rough and irregular) are observed, which are indicative of irreversible membranes damage.[65] Additionally, the color variation is characterized before and after the ILs application by spectrophotometric technique. The changes in the colorimetric values (*i.e.*, ΔE) of the sandstone samples coated with 10 mg mL^{-1} of $[P_{44412}][POM]$, $[P_{44414}][POM]$, and $[P_{66614}][POM]$ are 3.56, 3.36, and 4.6, respectively (Fig. S2†), showing no significant color changes and thus their potential as antifungal agents for heritage sandstones.

4. Conclusions

In summary, three phosphonium-based ILs, $[P_{44412}][POM]$, $[P_{44414}][POM]$, and $[P_{66614}][POM]$, were prepared and their thermal properties and *in vitro* antifungal activities against four dematiaceous fungi were evaluated. The results of fast-scan (10 °C min^{-1}) TGA method show that $[P_{66614}][POM]$, with longer alkyl chains, also exhibits lower thermal stability than $[P_{44412}][POM]$ and $[P_{44414}][POM]$, which may be due to the increased stability of the carbocation and/or carbon radicals when the alkyl chain increases. All three ILs have been shown to exhibit antifungal activity, but the resultant $[P_{44412}][POM]$ with shorter alkyl substituent has a much higher antifungal activity in comparison with $[P_{44414}][POM]$ and $[P_{66614}][POM]$, confirming that the optimized chain length of alkyl substitution on tetraalkylphosponium cation enhances the antifungal activity. More importantly, the application of ILs-based coatings on sandstone sample exhibits strong antifungal activity and no significant color changes, which makes it a promising candidate for the treatment of invasive fungi colonizing heritage sandstone. These results are preliminary and future studies will further investigate the antifungal performances of ILs under *in situ* conditions.

Conflicts of interest

There are no conflicts to declare.

Acknowledgements

This research is supported by National Natural Science Foundation of China (No. 31900104) and National Key Research and Development Program of China (2019YFC1520503).

References

1 O. Salvadori and A. Casanova, *Open Conf. Proc. J.*, 2016, **7**, 39–54.
2 S. Onofri, L. Zucconi, D. Isola and L. Selbmann, *Plant Biosyst.*, 2014, **148**, 384–391.

3 J. Trovao, A. Portugal, F. Soares, D. S. Paiva, N. Mesquita, C. Coelho, A. C. Pinheiro, L. Catarino, F. Gil and I. Tiago, *Int. Biodeterior. Biodegrad.*, 2019, **142**, 91–102.
4 G. Michael, J. Bahri-Esfahani, Q. W. Li, Y. J. Rhee, Z. Wei, M. Fomina and X. J. Liang, *Fungal Biol. Rev.*, 2014, **28**, 36–55.
5 K. Sterflinger, *Fungal Biol. Rev.*, 2010, **24**, 47–55.
6 J. M. De la Rosa, P. M. Martin-Sanchez, S. Sanchez-Cortes, B. Hermosin, H. Knicker and C. Saiz-Jimenez, *Sci Rep.*, 2017, **7**, 13441.
7 D. Isola, L. Selbmann, P. Meloni, E. Maracci, S. Onofri and L. Zucconi, in *Science and Technology for the Conservation of Cultural Heritage*, 2013, pp. 83–86, DOI: 10.1201/b15577.
8 C. Saizjimenez, *Sci. Total Environ.*, 1995, **167**, 273–286.
9 K. Sterflinger, D. Tesei and K. Zakharova, *Fungal Ecol.*, 2012, **5**, 453–462.
10 A. A. Gorbushina, K. Whitehead, T. Dornieden, A. Niesse, A. Schulte and J. I. Hedges, *Can. J. Bot.*, 2003, **81**, 131–138.
11 A. Thywißen, T. Heinekamp, H. M. Dahse, J. Schmaler-Ripcke, S. Nietzsche, P. F. Zipfel and A. A. Brakhage, *Front. Microbiol.*, 2011, **2**, 96.
12 F. Bastian and C. Alabouvette, *Int. J. Speleol.*, 2009, **38**, 55–60.
13 R. Almeida-Paes, M. H. G. Figueiredo-Carvalho, F. Brito-Santos, F. Almeida-Silva, M. M. E. Oliveira and R. M. Zancope-Oliveira, *Plos One*, 2016, **11**, e0152796.
14 C. Urzi and F. De Leo, *Int. Biodeterior. Biodegrad.*, 2007, **60**, 25–34.
15 M. R. Fidanza and G. Caneva, *J. Cult. Herit.*, 2019, **38**, 271–286.
16 P. Sanmartin, A. Rodriguez and U. Aguiar, *Int. Biodeterior. Biodegrad.*, 2020, **147**, 104870.
17 *Art, Biology and Conservation. Biodeterioration of Works of Art*, ed. M. P. Nugari, O. Salvadori, R.J. Kestler, V.H. Kestler, A.E. Charola and F.E. Nietto-Fernandez, The Metropolitan Museum of Art, New York, 2002, pp. 519–535.
18 M. Romani, T. Warscheid, L. Nicole, L. Marcon, P. Di Martino, M. T. Suzuki, P. Lebaron and R. Lami, *Sci. Total Environ.*, 2022, **802**, 149846.
19 I. Franco-Castillo, L. Hierro, J. M. de la Fuente, A. Seral-Ascaso and S. G. Mitchell, *Chem*, 2021, **7**, 629–669.
20 F. Palla, M. Bruno, F. Mercurio, A. Tantillo and V. Rotolo, *Molecules*, 2020, **25**, 730.
21 E. Semenzin, E. Giubilato, E. Badetti, M. Picone, A. V. Ghirardini, D. Hristozov, A. Brunelli and A. Marcomini, *Environ. Sci. Pollut. Res.*, 2019, **26**, 26146–26158.
22 M. Reyes-Estebanez, B. O. Ortega-Morales, M. Chan-Bacab, C. Granados-Echegoyen, J. C. Camacho-Chab, J. E. Pereanez-Sacarias and C. Gaylarde, *Heritage Sci.*, 2018, **6**, 52.
23 J. P. Hallett and T. Welton, *Chem. Rev.*, 2011, **111**, 3508–3576.
24 M. F. Pacheco, A. I. Pereira, L. C. Branco and A. J. Parola, *J Mater Chem A*, 2013, **1**, 7016–7018.
25 J. M. Delgado, D. Nunes, E. Fortunato, C. A. T. Laia, L. C. Branco and M. Vilarigues, *Corros. Sci.*, 2017, **118**, 109–117.
26 F. De Leo, P. Cardiano, G. De Carlo, S. Lo Schiavo and C. Urzì, *J. Mol. Liq.*, 2017, **248**, 81–85.
27 C. Croitoru and I. C. Roata, *Molecules*, 2020, **25**, 4289.
28 J. Pernak, I. Goc and A. Fojutowski, *Holzforschung*, 2005, **59**, 473–475.
29 N. Dimitric, N. Spremo, M. Vranes, S. Belic, M. Karaman, S. Kovacevic, M. Karadzic, S. Podunavac-Kuzmanovic, D. Korolija-Crkvenjakov and S. Gadzuric, *RSC Adv.*, 2019, **9**, 17905–17912.
30 K. Schmitz, S. Wagner, M. Reppke, C. L. Maier, E. Windeisen-Holzhauser and J. P. Benz, *Plos One*, 2019, **14**, e0219650.
31 S. Lo Schiavo, F. De Leo and C. Urzi, *Appl. Sci.*, 2020, **10**, 6568.
32 F. De Leo, A. Marchetta, G. Capillo, A. Germana, P. Primerano, S. Lo Schiavo and C. Urzi, *Coatings*, 2021, **11**, 26.
33 K. Rajkowska, A. Kozirog, A. Otlewska, M. Piotrowska, E. Atrian-Blasco, I. Franco-Castillo and S. G. Mitchell, *Molecules*, 2020, **25**, 5663.
34 K. S. Egorova and V. P. Ananikov, *J. Mol. Liq.*, 2018, **272**, 271–300.
35 Z. Q. Zheng, Q. M. Xu, J. N. Guo, J. Qin, H. L. Mao, B. Wang and F. Yan, *ACS Appl. Mater. Interfaces*, 2016, **8**, 12684–12692.
36 M. C. Jennings, K. P. C. Minbiole and W. M. Wuest, *ACS Infect. Dis.*, 2015, **1**, 288–303.
37 Y. Jeon, J. Sung, C. Seo, H. Lim, H. Cheong, M. Kang, B. Moon, Y. Ouchi and D. Kim, *J. Phys. Chem. B*, 2008, **112**, 4735–4740.
38 N. I. Gumerova and A. Rompel, *Chem. Soc. Rev.*, 2020, **49**, 7568–7601.
39 A. Bijelic, M. Aureliano and A. Rompel, *Chem. Commun.*, 2018, **54**, 1153–1169.
40 S. Herrmann, L. De Matteis, J. M. de la Fuente, S. G. Mitchell and C. Streb, *Angew. Chem., Int. Ed.*, 2017, **56**, 1667–1670.
41 A. Misra, I. F. Castillo, D. P. Muller, C. Gonzalez, S. Eyssautier-Chuine, A. Ziegler, J. M. de la Fuente, S. G. Mitchell and C. Streb, *Angew. Chem., Int. Ed.*, 2018, **57**, 14926–14931.
42 Y. Li, X. Wu, Q. Wu, H. Ding and W. Yan, *Dalton Trans.*, 2014, **43**, 13591–13595.
43 P. G. Rickert, M. P. Antonio, M. A. Firestone, K. A. Kubatko, T. Szreder, J. F. Wishart, M. L. Dietz and U. Dame, *J. Phys. Chem. B*, 2007, **111**, 4685.
44 L. Li, H. Zhou, F. Gai, X. Chi, Y. Zhao, F. Zhang and Z. Zhao, *RSC Adv.*, 2017, **7**, 13244–13249.
45 Y. Xue and H. Xiao, *J. Biomed. Mater. Res., Part A*, 2016, **104**, 747–757.
46 Y. Xue, Y. F. Pan, H. N. Xiao and Y. Zhao, *RSC Adv.*, 2014, **4**, 46887–46895.
47 A. Téazéa, G. Hervéa, R. G. Finke and D. K. Lyon, *α-, β-, and γ-Dodecatungstosilicic Acids: Isomers and Related Lacunary Compounds*, Wiley-Blackwell, 1990.
48 C. G. Pierce, P. Uppuluri, A. R. Tristan, F. L. Wormley, E. Mowat, G. Ramage and J. L. Lopez-Ribot, *Nat. Protoc.*, 2008, **3**, 1494–1500.
49 L. N. Xie, B. J. Zhang and Y. L. Hu, *Int. J. Archit. Herit.*, 2021, DOI: 10.1080/15583058.2021.1942591.
50 T. Qiu, Q. Y. Zeng and N. J. Ao, *Mater. Lett.*, 2014, **122**, 13–16.

51 Y. Chen, W. Q. Tan, Q. Li, F. Dong, G. D. Gu and Z. Y. Guo, *Int. J. Biol. Macromol.*, 2018, **113**, 1273–1278.
52 J. G. Huddleston, A. E. Visser, W. M. Reichert, H. D. Willauer, G. A. Broker and R. D. Rogers, *Green Chem.*, 2001, **3**, 156–164.
53 H. Tokuda, K. Hayamizu, K. Ishii, M. A. B. H. Susan and M. Watanabe, *J. Phys. Chem. B*, 2005, **109**, 6103–6110.
54 C. Maton, N. De Vos and C. V. Stevens, *Chem. Soc. Rev.*, 2013, **42**, 5963–5977.
55 M. Montanino, M. Carewska, F. Alessandrini, S. Passerini and G. B. Appetecchi, *Electrochim. Acta*, 2011, **57**, 153–159.
56 K. Tsunashima, S. Kodama, M. Sugiya and Y. Kunugi, *Electrochim. Acta*, 2010, **56**, 762–766.
57 P. G. Rickert, M. R. Antonio, M. A. Firestone, K. A. Kubatko and M. L. Dietz, *Dalton Trans.*, 2007, **5**, 529–531.
58 K. Michael and H. W. Regina, *J. Funct. Biomater.*, 2018, **9**, 4.
59 S. Y. Hu, C. C. Ma, F. Y. Zhan, Y. L. Cao, P. F. Hu and Q. Zhen, *Chem. Pap.*, 2017, **71**, 1323–1329.
60 A. Kanazawa, T. Ikeda and T. Endo, *Antimicrob. Agents Chemother.*, 1994, **38**, 945–952.
61 L. Chang, J. Wang, C. Y. Tong, L. Zhao and X. M. Liu, *J. Appl. Polym. Sci.*, 2016, **133**, 43689.
62 M. Bustelo, A. Pinazo, M. A. Manresa, M. Mitjans, M. P. Vinardell and L. Perez, *Colloids Surf., A*, 2017, **532**, 501–509.
63 S. Y. Choi, H. Rodriguez, A. Mirjafari, D. F. Gilpin, S. McGrath, K. R. Malcolm, M. M. Tunney, R. D. Rogers and T. McNally, *Green Chem.*, 2011, **13**, 1527–1535.
64 M. T. Garcia, I. Ribosa, L. Perez, A. Manresa and F. Comelles, *Colloids Surf., B*, 2014, **123**, 318–325.
65 M. Petkovic, D. O. Hartmann, G. Adamova, K. R. Seddon, L. P. N. Rebelo and C. S. Pereira, *New J. Chem.*, 2012, **36**, 56–63.